

# Subsidence and Exhumation Dynamics of Eclogites in the Yukon–Tanana Terrane, Canadian Cordillera: Petrological Reconstructions and Geodynamic Modeling

A. L. Perchuk\* and T. V. Gerya\*\*,\*\*

\**Institute of the Geology of Ore Deposits, Petrography, Mineralogy, and Geochemistry (IGEM),  
Russian Academy of Sciences, Staromonetnyi per. 35, Moscow, 119017 Russia  
e-mail: alp@igem.ru*

\*\**Institute of Experimental Mineralogy (IEM), Russian Academy of Sciences,  
Chernogolovka, Moscow oblast, 142432 Russia  
e-mail: taras@iem.ac.ru*

\*\*\**Geologisches Institut–ETH–Zürich, Sonneggstrasse 5,  
CH-8092, Zurich, Switzerland*

Received March 1, 2004

**Abstract**—Eclogites from the Faro area in the Yukon–Tanana high-pressure terrane, Canada, are characterized by a counterclockwise  $P$ – $T$  path. The major minerals of these rocks are garnet, omphacite, and quartz. The cores of concentrically zoned garnet grains contain chemical heterogeneities of different types: relict garnet microinclusions (which were produced before the prograde  $P$ – $T$  evolution of the rocks) and stringers (which developed under  $P$ – $T$  conditions close to the metamorphic peak). Geospeedometers based on these types of chemical heterogeneity were used to obtain discrete estimates for the evolution rates of the  $P$ – $T$  parameters during the prograde and retrograde metamorphic stages. The  $P$ – $T$  path and the corresponding temporal aspects of the evolution of the Faro eclogites are well reproduced by numerical simulations of the viscous flow of material in a self-organizing subduction channel during subduction onset. According to the model, the subduction channel evolved predominantly at the expense of the hanging-wall serpentinitized peridotite.

## INTRODUCTION

The thermal structure of a subduction zone depends on several physical parameters, such as subduction velocity and duration, the age of the downgoing plate, the rheological characteristics of the crustal and mantle rocks, and the intensity of mantle wedge hydration (Cloos, 1982; Dobretsov and Kirdyashkin, 1992; Peacock, 1990; Bostock *et al.*, 2002; Gerya *et al.*, 2002). Inasmuch as most of these parameters vary from one subduction zone to another, each thermal structure can be regarded as unique in certain aspects. This is, in turn, reflected in the diversity of the metamorphic  $P$ – $T$  paths of high-pressure rocks. The  $P$ – $T$  paths of eclogites from some subduction zones portrayed in Fig. 1 differ in absolute temperatures and pressures and show a fairly broad diversity of thermal gradients (the temperature/pressure ratio). Notable differences are also typical of the configurations of their  $P$ – $T$  paths: most of them are directed clockwise, although paths of the opposite direction are also possible. The geodynamic situation controls the durations of the  $P$ – $T$  evolution of a rock and its thermal (cooling and/or heating rate) and baric (exhumation and/or burial rate) history.

The temporal aspect of rock evolution in subduction and collision zones recently attracts more and more rapt attention of researchers. Pertinent information is recov-

ered using techniques of geospeedometry (Perchuk and Philippot, 2000; Dachs and Proyer, 2002), geochronology (Gebauer *et al.*, 1997; Duchene *et al.*, 1997; Rubatto *et al.*, 2001), or, more rarely, a combination of both (Philippot *et al.*, 2001). In this publication, we compare the results obtained by mineralogical geospeedometry and geodynamic simulations. The main criterion of the convergence of the results was the rates of temperature and pressure changes during the prograde and retrograde metamorphic stages in the Faro eclogites of the Yukon–Tanana Terrane, Canada, and in a certain virtual rock from the basaltic layer of the oceanic crust, whose  $P$ – $T$ – $t$  evolution was followed in a numerical experiment. We selected the Faro eclogites because garnet contained in these rocks shows different types of chemical heterogeneities, and the simulation of their partial homogenization allowed us to obtain discrete estimates for the timing of the prograde and retrograde metamorphic stages.

## FARO ECLOGITE FROM THE YUKON–TANANA TERRANE, CANADIAN CORDILLERA

### *Geological Overview (Literature Data)*

Eclogites and glaucophane schists occur in the polymetamorphic Yukon–Tanana Terrane at the western margin of the North American Platform (Erdmer and

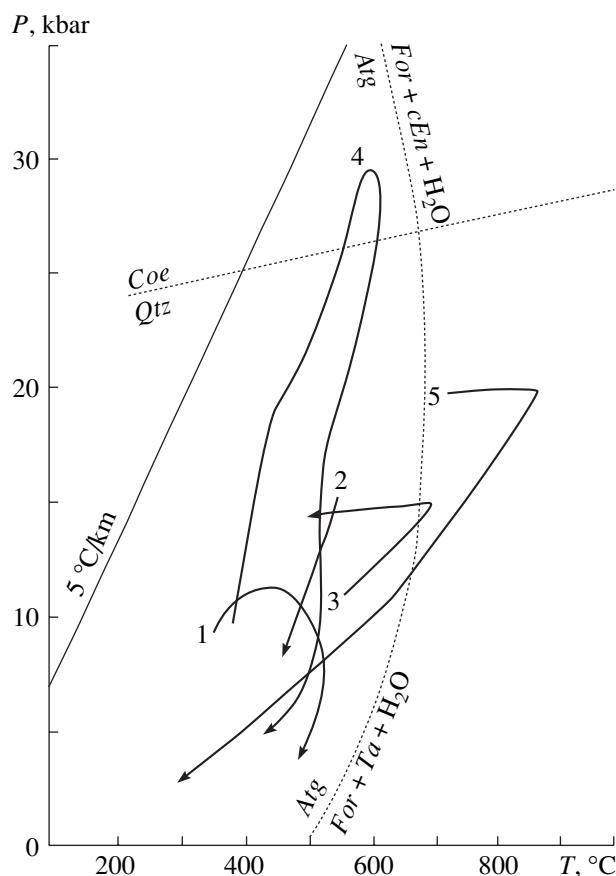


**Fig. 1.** Diversity of metamorphic  $P$ - $T$  paths of eclogite-facies rocks in subduction zones.

(1) New Caledonia (Ghent *et al.*, 1987); (2) Nerkau, Northern Urals (Gomez-Pugnaire *et al.*, 1997); (3) Faro, Yukon, Canada (Perchuk and Philippot, 2000); (4) Zermatt-Saas, Alps (Reinecke, 1998); (5) Sudety Mountains, Poland (Steltenpohl *et al.*, 1993). Mineral equilibria:  $Atg = For + cEn + H_2O$  (Wunder and Schreyer, 1997),  $Coe = Qtz$  (Bohlen and Boettcher, 1982). Mineral symbols: *Atg*—antigorite, *For*—forsterite, *cEn*—clinoenstatite, *Coe*—coesite, *Qtz*—quartz, *Ta*—talc.

Helmstaedt, 1983). The terrane is in tectonic contact with the platform: Mesozoic collision between the island arc and continent thrust this terrane over the sedimentary cover of the marginal part of the platform (Templeman-Kluit, 1979; Erdmer, 1987). The terrane comprises three allochthons (Erdmer and Helmstaedt, 1983), which consist of tectonized volcano-sedimentary rocks (Nisutlin allochthon), a cataclazed ophiolite association (Anvil), and cataclazed granitoids (Simpson). The Faro eclogites in the northern portion of the terrane belong to the Nisutlin allochthon and are part of tectonic melange in the subduction zone (Erdmer, 1987). In the Faro area, eclogites compose scarce lenses up to 4 m thick among graphite-bearing quartzites and blastomylonitized quartz-mica schists with garnet, chlorite, zoisite, calcite, and albite (Templeman-Kluit, 1979; Erdmer and Helmstaedt, 1983). The

schistosity of the eclogites and host rocks suggests their conformable relations, although the poor exposure of the terrane precludes determining the character of the contacts (Erdmer and Helmstaedt, 1983). Fairly scanty information on the geology of the Faro area is partly compensated by thorough descriptions of the neighboring Ross River area, which lies 45 km southeast of Faro (Fig. 2) and is part of the same Nisutlin allochthon (Erdmer, 1987). In the latter area, eclogites are hosted by graphite quartzites, quartz-muscovite-glaucophane-garnet and chlorite-actinolite-plagioclase schists and serpentinites. The eclogites have sharp contacts with their host rocks, often with graphite rims along the contacts (Erdmer, 1987). A geological map of this area is presented in Fig. 2, inset b.

The geochemistry of the Faro eclogites suggests (Philippot *et al.*, 2001) that their protolith consisted of oceanic-island basalts. The Permian age (252–264 Ma) of the eclogite metamorphism (Lu-Hf method; Philippot *et al.*, 2001) practically coincides with the age of phengite from the eclogite (255–261 Ma,  $^{40}\text{Ar}/^{39}\text{Ar}$  method; Erdmer *et al.*, 1998). The closure temperature of the isotopic system of the phengite is  $\sim 550^\circ\text{C}$  (Perchuk and Philippot, 2000), i.e., close to the  $P$ - $T$  conditions of the retrograde metamorphism.

The reader can find more information on the geology of the Yukon-Tanana Terrane in (Erdmer and Helmstaedt, 1983; Erdmer, 1987; Hansen *et al.*, 1991; Erdmer *et al.*, 1998).

#### *Petrography, Mineralogy, and Garnet Zoning*

The main rock-forming minerals of the petrographically freshest Faro eclogites are garnet, omphacite, and quartz. The rocks are porphyroblastic, schistose, and most of their garnet grains are euhedral. The idioblasts up to a few millimeters across bear numerous inclusions of quartz, omphacite, clinozoisite, and acicular rutile and more rare paragonite, phengite, and sphene. Inclusions are concentrated mostly in the cores of garnet grains, whose peripheral portions are much poorer in inclusions. The retrograde alterations are clearly pronounced only locally, where omphacite and quartz (anhydrous minerals) are virtually completely replaced by phengite + paragonite + amphibole + chlorite + clinozoisite aggregates (consisting exclusively of hydrous minerals). Garnet in the segregations is resorbed and surrounded by thin rims of chlorite and/or phengite. Note that both chlorite and phengite also occur, along with glaucophane, in the host garnet-mica schists, in which they are major rock-forming minerals (Erdmer and Helmstaedt, 1983).

The garnet has clearly pronounced concentric growth zoning (Fig. 3a), with cores enriched in Fe and Mn and rims richer in Mg. The cores of idioblasts sometimes include well pronounced domains of high-Ca garnet (Fig. 3b), which were interpreted as earlier-generation relicts (Perchuk and Philippot, 2000).

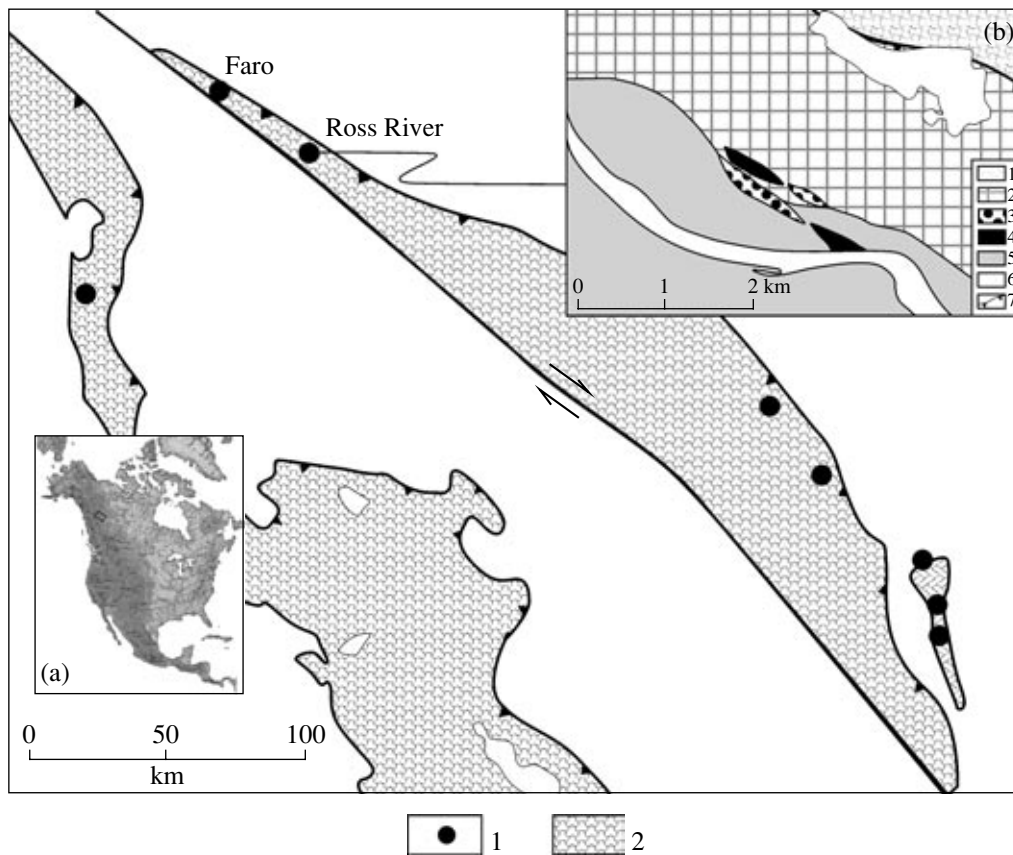


**Fig. 2.** Geological-geographic setting of eclogites in the Yukon-Tanana Terrane (Erdmer, 1987).

(1) Eclogite exposures; (2) Yukon-Tanana Terrane. Arrows correspond to the displacement directions of blocks along the Tintina fault. Insets: (a) Schematic index map of the North American continent and the Yukon-Tanana Terrane (rectangle); (b) schematic geological map of the Ross River area (modified after Erdmer, 1987). Symbols in inset (b): (1) platform sedimentary cover; (2) mylonitized mica schists and quartzites; (3) eclogites and glaucophane schists; (4) serpentinites; (5) greenschists; (6) rivers and lakes; (7) overthrust.

Garnet in high-pressure rocks sometimes preserves stringers, which are microcracks healed by newly formed garnet (Perchuk and Varlamov, 1995; Yapaskurt, 1997). Garnets from the Faro eclogites bear two generations of stringers (Figs. 3b–3d): (i) stringers that developed under the  $P$ – $T$  conditions close to the metamorphic peak and (ii) stringers produced after the metamorphic peak. In BSE images, the generation-1 stringers are dark and can be clearly seen in the pale gray garnet core (Figs. 3b, 3c). The generation-2 stringers are pale and can be readily distinguished in both the core and the margin of the garnet (Fig. 3d). Microprobe profiles across the stringers (Figs. 4a–4c) in different grain parts (Figs. 3c, 3d) reveal compositional differences between stringers of different generations and the host garnet. The generation-1 stringers have higher Mg content, and their composition is close to that of the rim, while the generation-2 stringers are more ferrous and, thus, are contrasting with the dark magnesian rim. Garnet analyses (table) were conducted on a CAMECA SX-100 microprobe at the Laboratory of Magma and Volcanoes of the University of Clermont-Ferrand,

France, at an accelerating voltage of 15 kV and a current of 15 nA. The beam diameter was 1  $\mu$ m. The standards were natural and synthetic compounds.

The genesis of the stringers is thought to have been related to the healing of microcracks (Perchuk and Varlamov, 1995; Yapaskurt, 1997) or diffusion along the boundaries of subgrains (Prior *et al.*, 2000). Now geospeedometry can be conducted only using stringers of the prograde stage (generation 1), which were produced under the  $P$ – $T$  parameters of the metamorphic peak. It is difficult to determine the exact age (and  $P$ – $T$  parameters) of the generation-2 stringers, because no minerals coexisting with them were identified.

The generation-1 stringers (Fig. 3b) were further examined on a scanning electron microscope at the Ruhr University in Bochum, Germany, by the electron backscatter diffraction (EBSD) technique. This technique did not reveal any boundaries of subgrains in a garnet crystal (S.Chakraborty, personal communication), and thus, we give preference to the mechanism of microcrack healing. Additional information on the petrography, mineralogy, and metamorphic zoning of

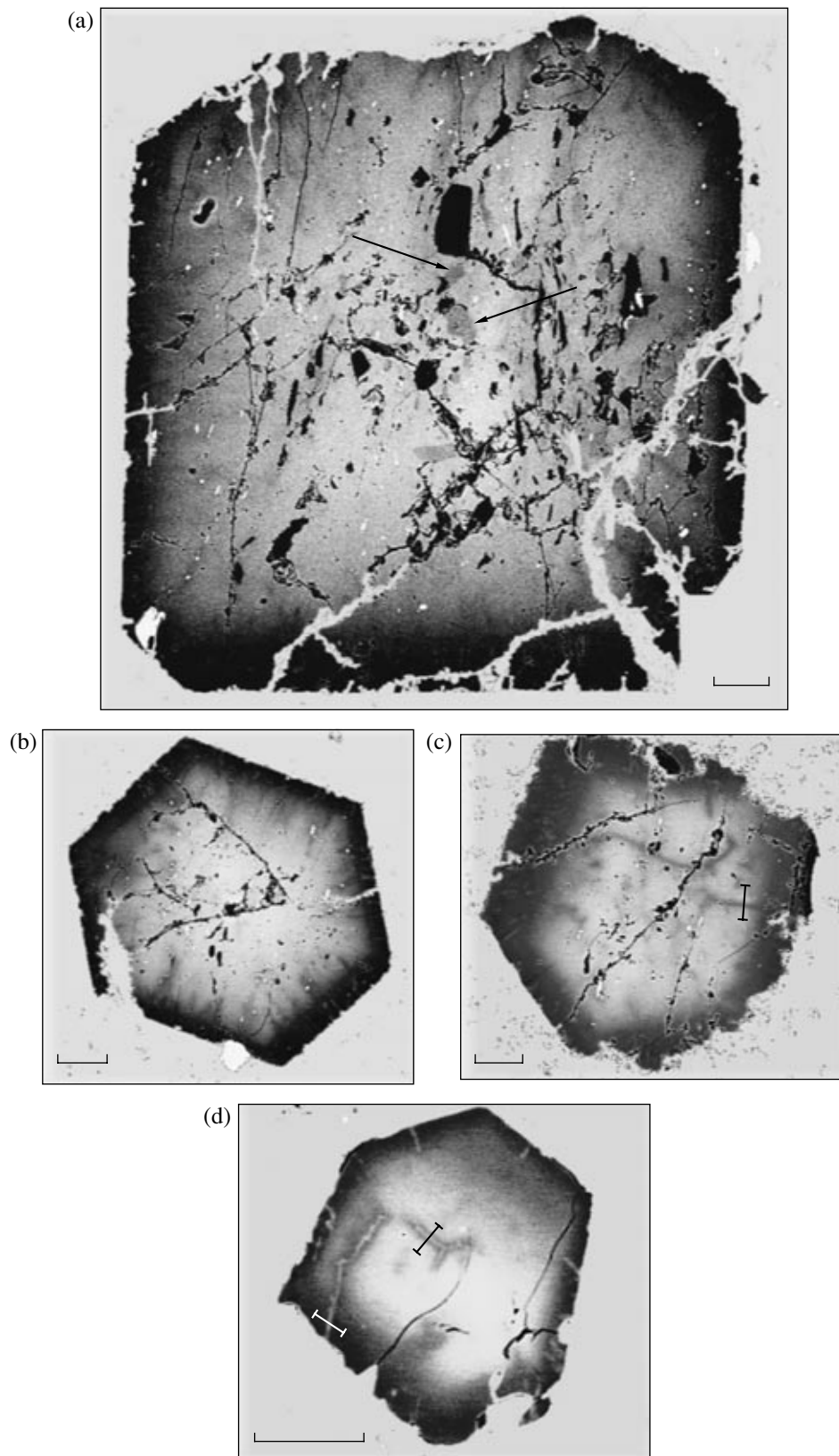


**Fig. 3.** BSE images of the principal types of garnet heterogeneities.

(a) Concentric growth zoning (pale core and darker margin) and garnet inclusions (indicated by arrows) in garnet; (b, c) stringers of the first generation; (d) stringers of the second generation (see text for details). Note that “post-growth” stringers typically have a pale stripe running across the stringer and rim. Figures 3c and 3d show the positions of microprobe profiles demonstrated in Fig. 4. Scale bars in all images are 100  $\mu\text{m}$  long.

eclogites from different parts of the Yukon–Tanana Terrane, including Faro, can be found elsewhere (Erdmer and Helmstaedt, 1983; Erdmer, 1987; Erdmer *et al.* 1998; Perchuk and Philippot, 2000).

#### Metamorphic $P$ – $T$ Conditions

The  $P$ – $T$  parameters of prograde metamorphism determined previously (Perchuk *et al.*, 1999; Perchuk and Philippot, 2000) were refined with a newly developed version of the garnet–clinopyroxene thermometer (Ravna, 2000). The pressure was evaluated by the clinopyroxene–plagioclase–quartz barometer (Perchuk, 1992) with a correction for plagioclase ordering (Salje, 1985). The calculations were conducted for the compositions of omphacite inclusions and their host garnet and the compositions of garnet margins and matrix omphacite in contact with them. We determined that the  $P$ – $T$  parameters of prograde metamorphism had increased from  $\sim 540^\circ\text{C}$  and 11 kbar to  $\sim 660^\circ\text{C}$  and 15 kbar. The subsequent cooling of the rock to  $\sim 540^\circ\text{C}$  proceeded under nearly isobaric conditions (Perchuk *et al.*, 1999; Perchuk and Philippot, 2000), as was inferred from the absence of clinopyroxene–plagioclase symplectites after omphacite and quartz, even in rock portions accessible to aqueous fluid (which acted as a catalyst of this reaction). The stable coexistence of omphacite and quartz during the retrograde metamorphic stage determines the general counterclockwise direction of the  $P$ – $T$  path (Fig. 5a).

Earlier we discussed the integrated affect of prograde and retrograde stages according to the degrees of the partial homogenization of garnet inclusions in garnet (Perchuk *et al.*, 1999; Perchuk and Philippot, 2000). Stringers developing under  $P$ – $T$  conditions close to the metamorphic culmination provide an independent estimate for the duration of the retrograde stage. Subtracting this value from the total time span of the metamorphic cycle, one can calculate the duration of the prograde stage. The procedure of determining the timing of the prograde and retrograde metamorphic stages is portrayed schematically in Fig. 5b. It is underlain by the simulation of the diffusion-controlled modification of zonal profiles across garnet grains.

#### DIFFUSION: NUMERICAL SIMULATIONS AND A NEW COMPUTER PROGRAM

Diffusion processes were studied using the DXL computer program, which enables simulating multi-component diffusion for spherical and Cartesian coordinates at any form of the temperature and pressure functions of time. The DXL program accounts for the dependence of the diffusion coefficient on the compo-

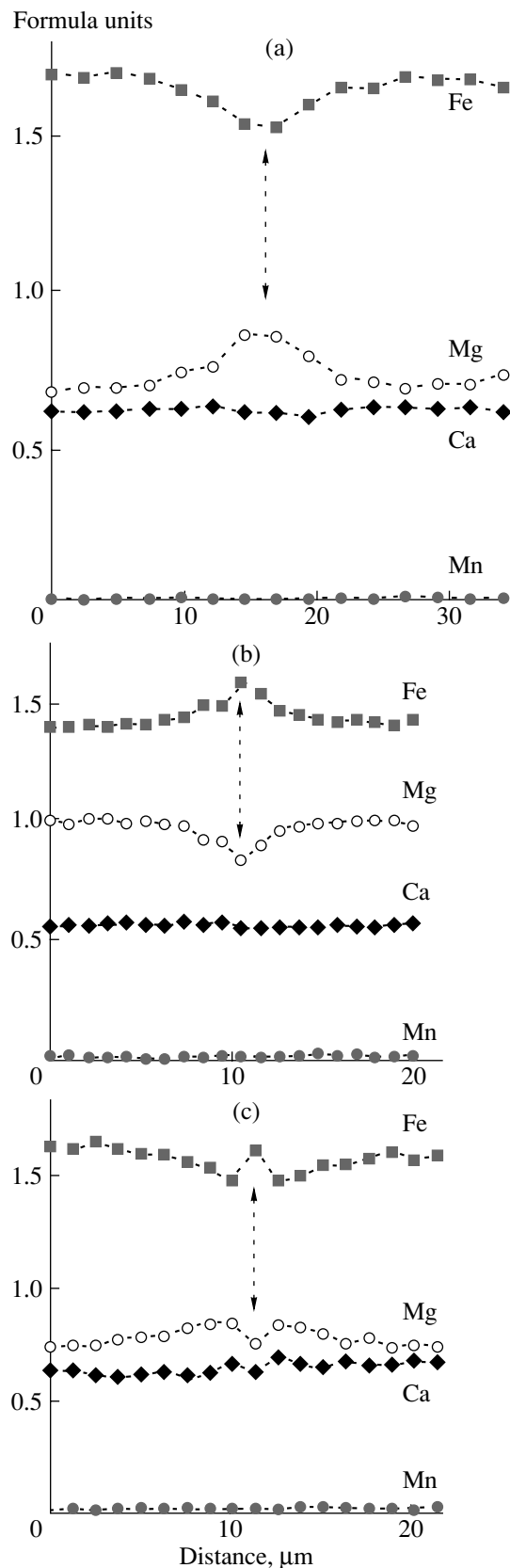


**Fig. 4.** Microprobe profiles across stringers of (a) the first and (b, c) second generations. Dashed lines mark the axis of the stringer. See Figs. 3c and 3d for the positions of the microprobe profiles.

Representative microprobe analyses of chemical heterogeneity domains in garnet

Component	Host garnet		Stringer (core)		Relic
	margin	core	retrograde	prograde	core
SiO <sub>2</sub>	39.09	38.41	38.35	38.68	37.95
TiO <sub>2</sub>	0.05	0.06	0.06	0.01	0.13
Al <sub>2</sub> O <sub>3</sub>	22.08	21.63	21.97	21.98	21.50
Cr <sub>2</sub> O <sub>3</sub>	0.02	0.04	0.02	0.17	0.02
FeO	22.73	25.38	25.28	24.37	21.26
MnO	0.27	0.27	0.36	0.32	5.47
MgO	8.96	6.42	6.51	7.56	1.17
CaO	6.89	8.09	7.57	7.32	12.60
Na <sub>2</sub> O	0.13	0.00	0.03	0.02	0.00
K <sub>2</sub> O	0.00	0.02	0.02	0.02	0.00
Total	100.21	101.00	100.16	100.45	100.09
12 atoms O					
Si	2.98	2.97	2.97	2.97	3.00
Al	1.98	1.97	2.00	1.99	2.00
Cr	0.00	0.00	0.00	0.01	0.00
Ti	0.00	0.00	0.00	0.00	0.01
Fe <sup>3+</sup>	0.04	0.05	0.03	0.04	0.00
Fe <sup>2+</sup>	1.41	1.59	1.61	1.53	1.41
Mn	0.02	0.02	0.02	0.02	0.37
Mg	1.02	0.74	0.75	0.86	0.14
Ca	0.56	0.67	0.63	0.60	1.07
Na	0.02	0.00	0.00	0.00	0.00
K	0.00	0.00	0.00	0.00	0.00
Total	8.00	8.01	8.01	8.01	7.99
X <sub>Mg</sub> <sup>*</sup>	0.42	0.32	0.32	0.36	0.09
X <sub>Ca</sub> <sup>**</sup>	0.19	0.22	0.21	0.20	0.36

\* X<sub>Mg</sub> = Mg/(Mg + Fe<sup>2+</sup>).  
 \*\* X<sub>Ca</sub> = Mg/(Ca + Mg + Fe<sup>2+</sup>).

sition and is applicable to any type of zoning profiles. Incorporating the program into a Microsoft Excel spreadsheet simplifies its use and opens broad possibilities for the graphical representation of the results. DXL optimizes a well-known mathematic apparatus for the simulation of multicomponent diffusion (see, for example, Toor, 1964; Lasaga, 1979). No corrections for the nonideality of the garnet solid solution were introduced, because this effect practically does not affect the results (Chakraborty and Ganguly, 1992).

In multicomponent diffusion, the flux of each cation in a mineral depends on the concentration gradients of the other cations with linear coefficients, which are specified in a matrix of diffusion coefficients  $D_{ij}$ . When the diffusion coefficients  $D_{ij}$  depend on the composi-

tion, the Fick–Onsager relation (Onsager, 1945) acquires the form

$$\frac{\partial C_i}{\partial t} = \frac{\partial}{\partial x} \sum_j^{n-1} D_{ij} \left( \frac{\partial C_j}{\partial x} \right), \quad (1)$$

where  $C_i$  is the mole fraction of the component in a  $n$ -component system, and  $x$  is the distance. For example, for the situation with three components (Fe, Mg, and Mn), a system of two equations can be written

$$\frac{\partial C_{\text{Fe}}}{\partial t} = \frac{\partial}{\partial x} \left( D_{\text{FeFe}} \left( \frac{\partial C_{\text{Fe}}}{\partial x} \right) + D_{\text{FeMg}} \left( \frac{\partial C_{\text{Mg}}}{\partial x} \right) \right);$$

$$\frac{\partial C_{\text{Mg}}}{\partial t} = \frac{\partial}{\partial x} \left( D_{\text{MgFe}} \left( \frac{\partial C_{\text{Fe}}}{\partial x} \right) + D_{\text{MgMg}} \left( \frac{\partial C_{\text{Mg}}}{\partial x} \right) \right).$$

The concentration of the third component (Mn) is thereby assumed to be dependent on the Fe and Mg concentrations. Expression (1) for a spherical crystal can be written as (Crank, 1975)

$$\frac{\partial C_i}{\partial t} = \frac{1}{r^2} \frac{\partial}{\partial r} \sum_j^{n-1} D_{ij} r^2 \left( \frac{\partial C_j}{\partial r} \right), \quad (2)$$

where  $r$  is the radial position in the crystal.

In application to the diffusion matrix  $D$  of an ionic crystal, Lasaga (1979) proposed the expression

$$D_{ij} = D(i) \delta_{ij} - \left[ D(i) z_i z_j C_i / \sum_{k=1}^n z_k^2 C_k D(k) \right] (D(j) - D(n)), \quad (3)$$

where  $\delta_{ij} = 0$  at  $i \neq j$  and  $\delta_{ij} = 1$  at  $i = j$ ,  $z$  is the charge of the component, and element  $n$  is regarded as dependent. The selfdiffusion coefficient  $D(i)$  of component  $i$  is described by the Arrhenius equation

$$D(i) = D_0 \exp \left( \frac{-E_a}{RT(t)} \right), \quad (4)$$

where  $D_0$  is a preexponential factor,  $E_a$  is the activation energy,  $P$  is pressure,  $R$  is the gas constant, and  $T(t)$  is temperature as a function of time.

The analytical solution of problems with multicomponent diffusion in minerals (1–3) is usually achieved by introducing components for which the matrix of diffusion coefficients is a diagonal matrix (see, for example, Loomis *et al.*, 1985; Chakraborty, 1991; Perchuk *et al.*, 1996). They are used for a transition to a matrix of standard diffusion equations. However, many petrological and geochemical problems are not isothermal in essence. Moreover, the diffusion coefficients of minerals (garnet among others) can be dependent on the concentration (see, for example, Gerasimov, 1987). The solution of such problems is further complicated by the fact that changing diffusion matrix (3) requires recalculations during each time step. To simplify the solution,

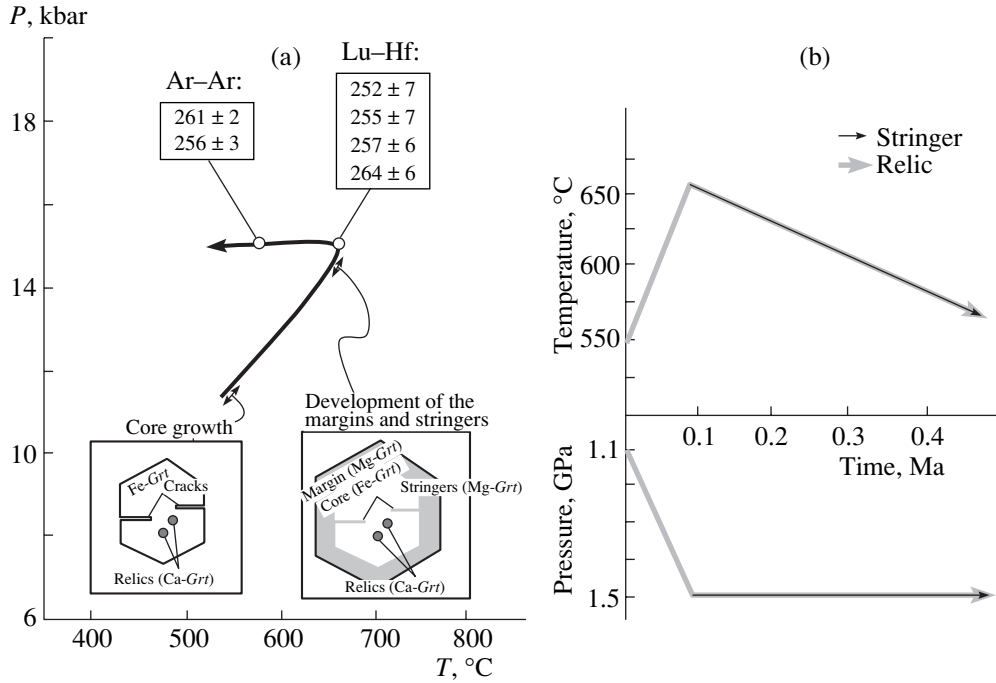


**Fig. 5.** (a) *P*–*T* evolution of the Faro eclogites, Yukon, Canada (modified after Perchuk *et al.*, 1999) and stages when different garnet heterogeneities were formed. The radiogenic ages (Ma) are given according to (Erdmer *et al.*, 1998; Philippot *et al.*, 2001). (b) Schematic variations in the pressure (*P*) and temperature (*T*) with time and their correlation with the data of geospeedometry. Shown in gray is the proposed formation time of stringers.

Chakraborty and Ganguly (1991) proposed an isothermal approximation, in which characteristic temperature  $T_x = 0.97T_{\text{peak}}$  (where  $T_{\text{peak}}$  is the temperature of the metamorphic peak in K) is introduced instead of the temperature change during the prograde and retrograde stages. Leaping ahead, it is pertinent to mention that this approximation leads to notable deviations from the nonisothermal solution in application to the Faro eclogites, which are characterized by asymmetrical *T*–*t* and *P*–*T* evolutionary trajectories (both prograde and retrograde).

The simulations were conducted using conservative finite-difference (FD) scheme over an irregularly-spaced staggered grid. The difference schemes were written in an implicit form for using the integration–interpolation technique from (Kalitkin, 1978). In an orthogonal system, one-dimensional diffusion equation (1) was written as

$$\frac{(C_n^{m+1} - C_n^m)}{t_{m+1} - t_m} = \frac{2}{(x_{n+1} - x_{n-1})} \times \left( \frac{D_{n+1/2}^{m+1}(C_{n+1}^{m+1} - C_n^{m+1})}{(x_{n+1} - x_n)} - \frac{D_{n-1/2}^{m+1}(C_n^{m+1} - C_{n-1}^{m+1})}{(x_n - x_{n-1})} \right), \quad (5)$$

where *n* and *m* are grid nodes for variables *x* and *t*, respectively.

In a spherical system of coordinates, expression (2) was replaced by a difference scheme

$$\frac{(C_n^{m+1} - C_n^m)}{t_{m+1} - t_m} = \frac{1}{r_n^2(r_{n+1} - r_{n-1})} \times \left( \frac{D_{n+1/2}^{m+1}(C_{n+1}^{m+1} - C_n^{m+1})(r_{n+1} + r_n)^2}{2(r_{n+1} - r_n)} - \frac{D_{n-1/2}^{m+1}(C_n^{m+1} - C_{n-1}^{m+1})(r_{n-1} + r_n)^2}{2(r_n - r_{n-1})} \right). \quad (6)$$

The difference equations were solved by introducing the initial distribution of element concentrations along the diffusion profile

$$C_n^0 = \mu(x_n)$$

and the condition that the system is closed (symmetrical) at its boundaries

$$C_0^m = C_1^m; \quad C_n^m = C_{n-1}^m.$$

The systems of equations were solved by the Gauss elimination method. To obtain a stable solution, the time step  $\Delta t$  was chosen to be dependent on the distance step  $\Delta x$  and the diffusion coefficient *D*, in compliance with the expression  $\Delta t \leq 1/2 \Delta x^2/D$  (Peacock, 1990).

Following the conventional praxis (Loomis *et al.*, 1985), the program was tested by an analytical solution for a diffusion coefficient linearly dependent on com-

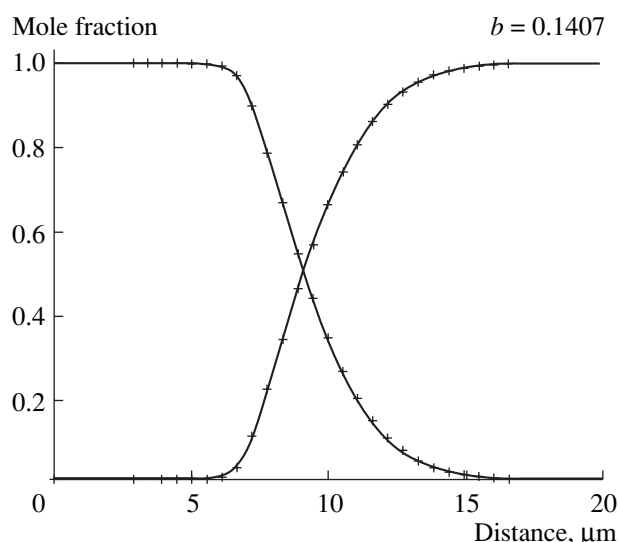


**Fig. 6.** Comparison between diffusion profiles obtained analytically (crosses) (Crank, 1975, pp. 118, 386) and by numerical simulations (lines) for diffusion between two semi-infinite rods of discrete compositions ( $C_1$  and  $C_2$ ) at a linear dependence of the diffusion coefficients on the concentration ( $b = 0.1407$  is the ratio of the diffusion coefficients at  $C_1$  and  $C_2$ ). The self-diffusion coefficient  $D_{\text{FeMg}}$  is calculated by the model (Darken, 1948). See text for details.

position (Crank, 1975, p. 118). The comparison of the numerical and analytical solutions for the situation with a strong dependence of the diffusion coefficient on composition (Crank, 1975, p. 386, Table 7.5,  $b = 0.1407$ , where  $b$  is the ratio of the diffusion coefficients for the marginal compositions) demonstrates a good consistency of the results.

#### CALCULATION OF TEMPORAL RELATIONS DURING METAMORPHISM

The timing of the prograde and retrograde metamorphic stages in the Faro eclogites were determined according to the scheme shown in Fig. 5.

#### Stringers

The compositions of stringers were used to evaluate the duration of the prograde stage. The methods for calculating temporal relations during metamorphism were described in (Perchuk and Philippot, 2000; Perchuk, 2002). The analytical solution used previously in application to eclogites from Norway and the Greater Caucasus was replaced by a numerical solution, and we additionally introduced a dependence of the diffusion coefficient on the garnet composition [Eq. (5) in the XXL computer program]. The transition from a stringer to the host garnet is determined by changes in the contents of two components: Fe and Mg, and, thus, we considered diffusion to be a binary process. The corre-

sponding diffusion coefficients for Eq. (4) were taken from (Ganguly *et al.*, 1998): Mg [ $D_0 = 4.66 \times 10^{-9}$  m<sup>2</sup>/s and  $E_a$  (kJ/mol) = 254 + 0.53P (kbar)]; Fe [ $D_0 = 3.5 \times 10^{-9}$  m<sup>2</sup>/s and  $E_a$  (kJ/mol) = 274 + 0.56P (kbar)]. The initial composition of the stringers was assumed equal to the composition of the garnet rim ( $N_{\text{Mg}} = 40$ ), and the composition of the host garnet ( $N_{\text{Mg}} = 29$ ) was determined in the microprobe profile segment not affected by diffusion. The width of the stringer was selected in such a way that a microprobe profile across this stringer could be simulated. The simulated profile (Fig. 7a) for the monotonous cooling of the rock from 660 to 540°C at  $P = 15$  kbar during 0.36 m.y. exhibits a good agreement with the observed distribution of the components in the microprobe profile (Fig. 4a). The extent of the diffusion profile modification notably decreases with decreasing temperature (Fig. 7a) and becomes negligibly small at temperatures below 570°C.

#### Inclusions of Relict Garnet Grains

The overall duration of metamorphism was reconstructed using the degree of homogenization of earlier-generation garnet inclusions in the host garnet (Perchuk and Philippot, 2000). We applied a numerical solution of the diffusion equation for a sphere (2) to a nonisothermal situation with fluxes of three components: Ca, Fe, and (Mg + Mn). The Mn and Mg concentrations in the garnet vary relatively little and show similar profiles of chemical zoning (Fig. 7b). Because of this and for simplifying the solution, we combined both elements and regarded them as a single element Mg. The aforementioned self-diffusion coefficients of Fe and Mg (Ganguly *et al.*, 1998) were substituted into the  $D$  matrix of Eq. (3), along with the diffusion coefficient for Ca [ $D_0 = 7.2 \times 10^{-16}$  m<sup>2</sup>/s and  $E_a$  (kJ/mol) = 155 + 0.6P(kbar)] from (Schwandt *et al.*, 1996). Ca was considered to be an additional component, and its diffusion activation volume was assumed to be equal to that of Mn (Ganguly *et al.*, 1998).

The partial homogenization of the garnet inclusion in garnet continued during the prograde (540°C/11 kbar → 660°C/15 kbar) and retrograde (660°C/15 kbar → 570°C/15 kbar) metamorphic stages. As follows from our simulations of stringer homogenization, the duration of the latter stage was close to 0.36 m.y. The next task was to evaluate the timing of the prograde stage for which the simulated curves of the element concentrations in garnet would reproduce the microprobe profile (Fig. 7b). The lines correspond to a prograde stage that lasted for 0.08 m.y. and a subsequent episode of subsobaric cooling for 0.36 m.y. (Fig. 7b). Thus, the overall duration of metamorphism with effective mass transfer was about 0.44 m.y. Note that the method of isothermal approximation ( $T_x = 0.97T_{\text{max}}$ ; Chakraborty and Ganguly, 1991) yields a much lower overall durations of these events, equal to 0.24 m.y.

It is pertinent to consider more closely the dynamics of changes in the diffusion profile across the garnet

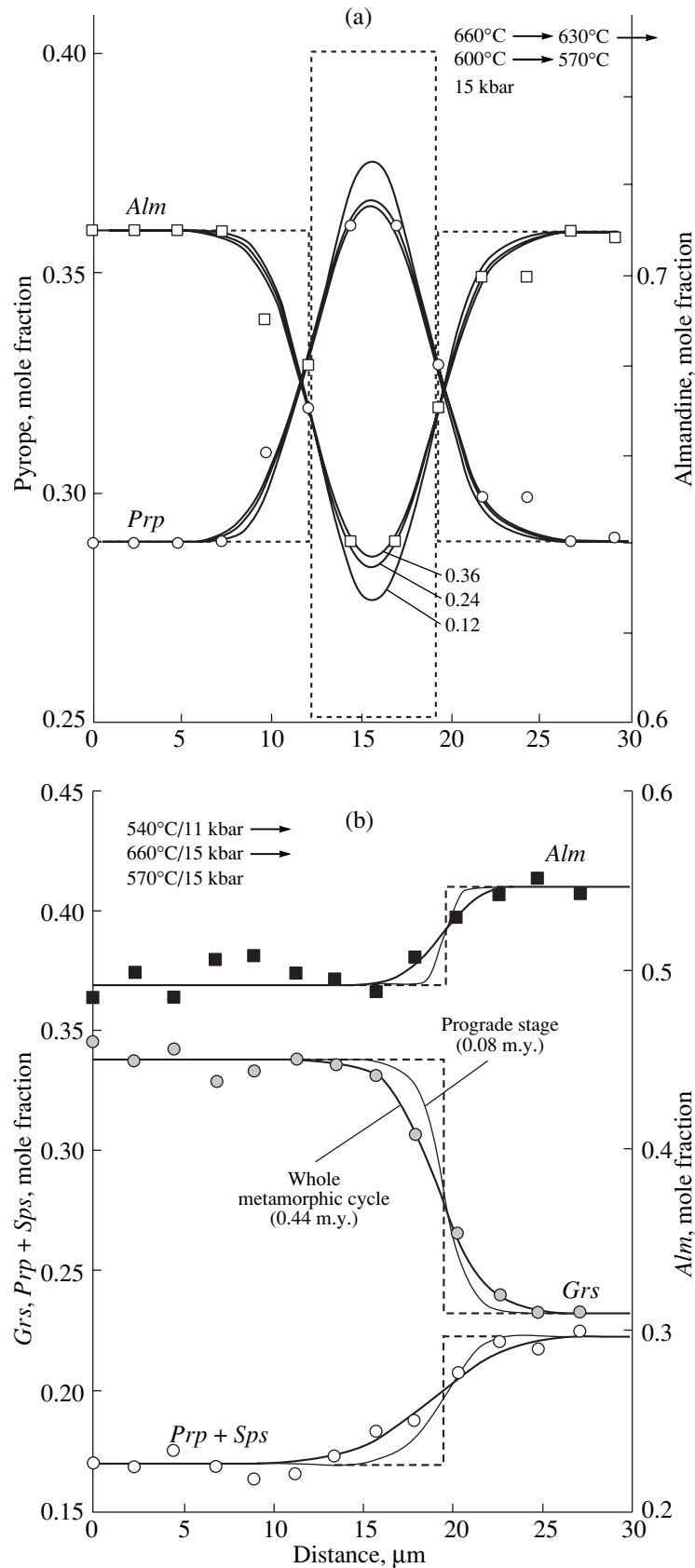


**Fig. 7.** Simulated diffusion modification of growth zoning.

(a) Stringer (Fig. 3a) was assumed as a semi-infinite plate; (b) spherical garnet inclusion (Perchuk and Philippot, 2000, Fig. 8). Dashed lines correspond to the initial profiles, numerals correspond to the time spans (m.y.) during which the diffusion profile developed.

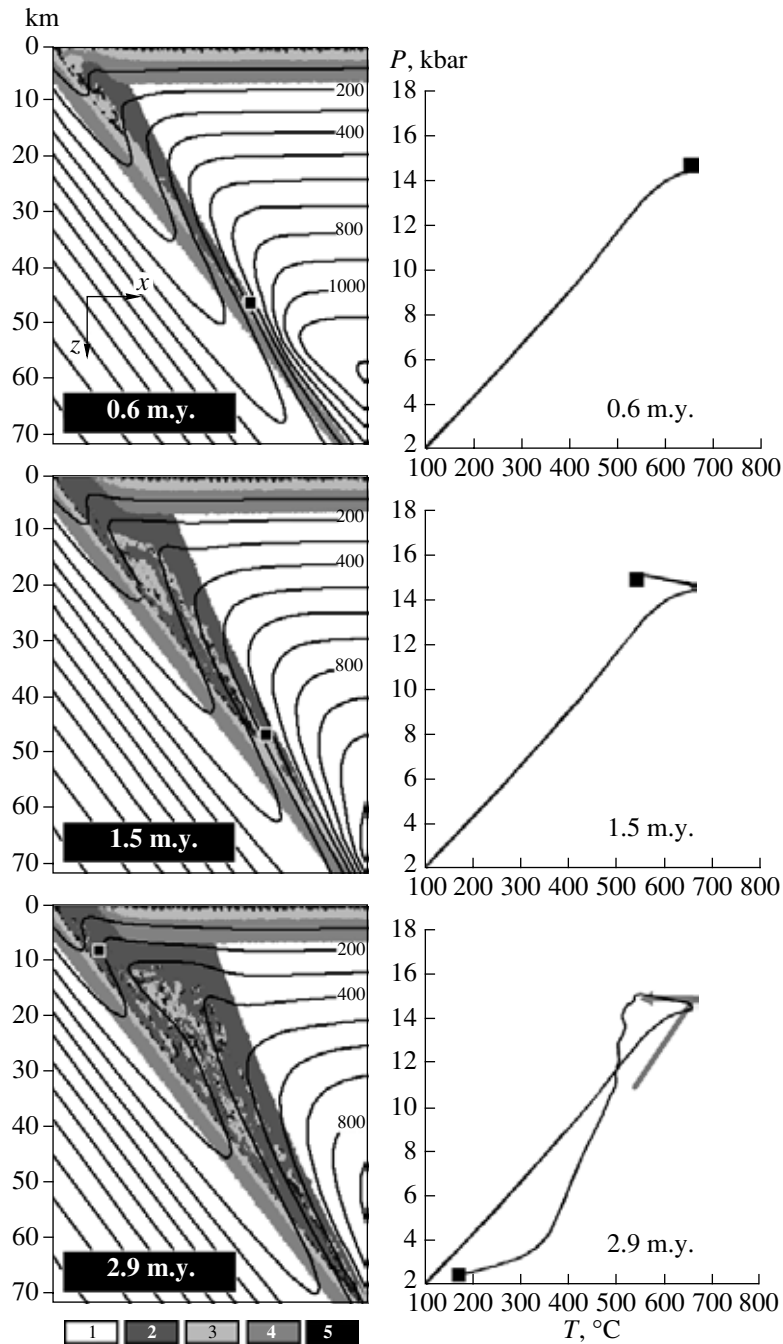


**Fig. 8.** Successive evolutionary stages of a subduction channel (a wedge-shaped region above the subducting plate) and the flow of low-viscosity material (serpentinized peridotites, metasediments, and eclogites in this channel). A metamorphic  $P$ - $T$  path for the eclogite body (square marker) in the frontal (deepest) portion of the subduction channel is presented for each stage. The last diagram additionally displays a metamorphic  $P$ - $T$  path for the Faro eclogite (gray arrow).

(1) Anhydrous mantle; (2) serpentinized mantle; (3) (meta)basalts; (4) (meta)gabbro; (5) (meta)sediments. Convergence velocity is 15 cm/yr. The computer program, together with the rheological and kinematic parameters used in it, is described in (Gerya *et al.*, 2002).

inclusion in garnet. First, effective mass transfer started during the prograde stage at a temperature of  $\sim 540^{\circ}\text{C}$  and ended at  $\sim 570^{\circ}\text{C}$  during the retrograde stage. Second, similar transformations of the profiles over analogous temperature intervals occurred much more rapidly during the prograde than the retrograde stages (the ratio of the time spans is approximately 1 : 5, Fig. 7b). In

other words, the rate of the diffusion smoothing the zonal profile during the prograde stage is much higher than the rate during the retrograde stage. The reason for these differences is the maximum concentration gradient at the interface of the garnets of contrasting compositions that existed only early in the course of the diffusion process.

Based on data on the prograde stage duration (0.08 m.y.) and the corresponding changes in the pressure (~4 kbar) and temperature (~120°C), one can easily evaluate the subduction velocity and the cooling rates, which were ~150 km/m.y. and 1500°C/m.y., respectively. Analogous calculations for the isobaric cooling stage yield a cooling rate of about 250°C/m.y. In the next section of this paper, these estimates will be compared with the results of numerical simulations of the viscous flow of material in the subduction channel.

#### NUMERICAL SIMULATION OF ECLOGITE EXHUMATION IN THE SUBDUCTION CHANNEL

The transportation mechanism of high-pressure rocks to the surface by the viscous return flow of metasediments in the subduction channel was explored for more than two decades (Hsu, 1971; Cloos, 1982; Dobretsov and Kirdyashkin, 1992; Gerya and Stoeckert, 2002). An approach recently applied to the solution of this problem is the 2D numerical simulation of a self-organizing accretionary prism and a subduction channel, with their morphology changing in accordance with the evolution of the thermal and petrological structures of the subduction zone (Gerya *et al.*, 2002). According to this model, the subduction channel filled with low-viscosity highly plastic hydrated crustal and mantle rocks (such as metasediments, eclogites, and serpentinites) is created not only due to the filling of the interplate zone with metasediments but also owing to the dehydration and serpentinization of the overlying mantle rocks (the mantle wedge or the hanging wall). Recent geophysical data indicate that mantle-wedge serpentinization is indeed a large-scale process (Bostock *et al.*, 2002). An analogous conclusion was drawn from structural and geochemical evidence on Himalayan serpentinites (Guillot *et al.*, 1999). The fluid for hydration and serpentinization of the mantle is derived from hydrous minerals in the downgoing oceanic plate, such as amphibole, chlorite, and epidote (Tatsumi, 1991; Ernst *et al.*, 1998; Schmidt and Poli, 1998). Serpentinization significantly changes the rheology of the rigid mantle rocks: according to recent experimental data, 10% serpentinized dunite has a strength equal to that of pure serpentinite (Escartin *et al.*, 2001). This effect seems to play a decisive role in the self-organization of the viscous return flow in the subduction channel, which is generated during the serpentinization of the hanging-wall peridotite and filled with serpentinites, metasediments, and eclogites (Fig. 8).

The metamorphic rocks composing the upper, most strongly hydrated plastic layer of the oceanic crust can be detached from the downgoing plate at depths of a few dozen kilometers (Fig. 8) and then be brought to the surface by the return flow in the subduction channel. These rocks can have different spatiotemporal trajectories and, accordingly, different  $P$ - $T$  paths (Gerya *et al.*, 2002). The results of simulation of this earliest subduction stage (Fig. 8), to which the Faro eclogites are likely

to be related (Perchuk and Philippot, 2000), deserve a closer consideration. Recall that these eclogites are characterized by a counterclockwise  $P$ - $T$  path, which is very unusual for this rock type. Our simulation demonstrates (Fig. 8a) that this configuration of the  $P$ - $T$  path is characteristic of rocks that occurred in the frontal (deep) part of the subduction channel during onset of subduction. The channel is very narrow there, and the return flow of rocks has not begun yet, but isotherms are significantly shifted to a deeper level, together with the downgoing cool plate. The deep part of the channel, where eclogites occur, is cooled, and this process continues until the subduction channel is widened to a size sufficient for the return flow to begin, which brings the rocks back to the surface (Fig. 8b). Thus, the unusual counterclockwise  $P$ - $T$  trajectory is caused not so much by the displacement of the rocks as by a change in the thermal structure of the subduction zone.

Using markers makes it possible to determine the trajectory, temperature, and timing of the displacement of rocks in the course of numerical experiment (Gerya and Stoeckert, 2002; Gerya *et al.*, 2002). For example, the  $P$ - $T$ - $t$  history of the Faro eclogites is realistically reproduced under the following conditions: a convergence velocity equal to 15 cm/yr at the subduction of a 40 Ma oceanic plate at an angle of 60° (Fig. 8). Numerical simulations demonstrate that the temperature and pressure vary nearly linearly with time during the evolution of the rock (marker) (Fig. 9). This observation validates the selection of the temperature and pressure dependences on time that were utilized in our simula-

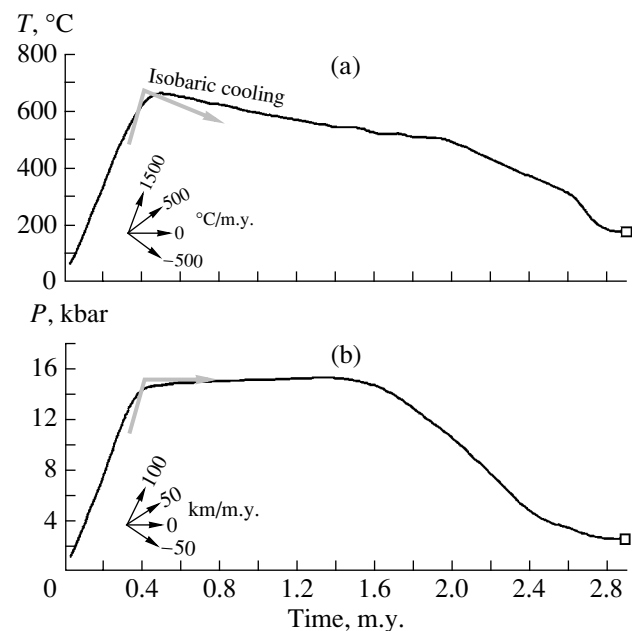


**Fig. 9.** Variations in (a) the temperature and (b) pressure with time for the marker (Fig. 7) that evolves during subduction initiation. Note that the temperature and pressure vary almost linearly. Arrows indicate  $T$ - $t$  and  $P$ - $t$  evolutionary paths for the Faro eclogites, Yukon-Tanana Terrane.

tions of garnet homogenization. The comparison of the results of the numerical simulations (Fig. 9) with petrological reconstructions for the Faro eclogites (Perchuk and Philippot, 2000) exhibits good qualitative and quantitative agreement: both yield similar  $P$ - $T$  paths, very high rates of changes of these parameters during the prograde stage (heating with a rate of  $1500^{\circ}\text{C}/\text{m.y.}$  and subduction with a velocity of  $140\text{ km}/\text{m.y.}$ ) and notably lower cooling rates under subsobaric conditions ( $\sim 250^{\circ}\text{C}/\text{m.y.}$ ). Now models are developed for the situation of subduction beneath an oceanic arc and/or continent with regard for the dynamics of erosional processes and sedimentation (see, for example, Gerya and Yuen, 2003). These models will make it possible to consider more closely the evolution of rocks at shallower exhumation levels (in accretionary prism), where the predominant rock type is metasediments instead of serpentinites (Cloos, 1982).

### CONCLUSIONS

The method for the reproduction of the temporal aspect of  $P$ - $T$  rock evolution on the basis of the original growth zoning of garnet is subject to further development. This paper is the first to demonstrate that this method offers the possibility of obtaining discrete estimates for the rates of temperature and pressure variations during different stages of the metamorphic evolution of rocks. For the eclogites of the Yukon-Tanana Terrane, it is established that the durations of the prograde ( $540^{\circ}\text{C}/11\text{ kbar} \rightarrow 660^{\circ}\text{C}/15\text{ kbar}$ ) and retrograde (subsobaric cooling from  $660^{\circ}\text{C}$  to  $570^{\circ}\text{C}$  at  $\sim 15\text{ kbar}$ ) stages were  $\sim 0.08$  and  $0.36\text{ m.y.}$ , respectively. The simulations were conducted by a newly developed program, which allows modeling multicomponent diffusion under nonisothermal conditions using a Microsoft Excel spreadsheet to make it much easier for the user to work with the program and visualize the results. The numerical simulation of a spontaneously evolving subduction channel reveals the distinctive features of the origin and exhumation of eclogites during the onset of subduction. The satisfactory agreement of the results of the numerical simulations with the  $P$ - $T$  path and the rates of temperature and pressure variations during the metamorphic evolution of the Faro eclogites can be regarded as evidence that the viscous flow of material in a subduction channel is the main mechanism maintaining eclogite displacement in the subduction zone.

### ACKNOWLEDGMENTS

The authors thank A.V. Gernis, S.P. Korikovskiy (Institute of the Geology of Ore Deposits, Petrography, Mineralogy, and Geochemistry, Russian Academy of Sciences), and L.L. Perchuk (Moscow State University) for valuable comments on the manuscript. W.V. Maresch (Ruhr-Universitaet, Bochum), P. Philippot (IPGP, Paris), and D. Vilzeuf (Universite Blais Pas-

cal, Clermont-Ferrand) are thanked for discussing the results and help with analytical studies. Rock samples for this research were made available by courtesy of P. Philippot (IPGP, Paris). This study was financially supported by A. von Humboldt Foundation, Germany, the Russian Foundation for Basic Research (project nos. 01-05-64585, 03-05-64633, and 1645.2003.5), the Deutsche Forschungsgemeinschaft (DFG, SFB Ruhr-Uni, Bochum), and the Swiss Federal Institute of Technology, Zurich (ETH Research Grant TH-12/04-1).

### REFERENCES

1. S. R. Bohlen and A. L. Boettcher, "The Quartz-Coesite Transformation: A Pressure Determination and the Effects of Other Components," *J. Geophys. Res.* **87**, 7073-7078 (1982).
2. M. G. Bostock, R. D. Hyndman, S. Rondenay, and S. M. Peacock, "An Inverted Continental Moho and Serpentinization of the Forearc Mantle," *Nature* **417**, 536-537 (2002).
3. S. Chakraborty and J. Ganguly, "Cation Diffusion in Aluminosilicate Garnets: Experimental Determination in Spessartine-Almandine Diffusion Couples, Evaluation of Effective Binary Diffusion Coefficients, and Applications," *Contrib. Mineral. Petrol.* **8**, 121-175 (1992).
4. S. Chakraborty and J. Ganguly, "Compositional Zoning and Cation Diffusion in Garnets," *Adv. Phys. Geochem.* **111**, 74-86 (1991).
5. M. Cloos, "Flow Melanges: Numerical Modeling and Geologic Constraints on Their Origin in the Franciscan Subduction Complex, California," *Geol. Soc. Am. Bull.* **93**, 330-345 (1982).
6. J. Crank, *The Mathematics of Diffusion* (Oxford Univ. Press, Oxford, 1975).
7. E. A. Dachs and A. Proyer, "Constraints on the Duration of High-Pressure Metamorphism in the Tauern Window from Diffusion Modeling of Discontinuous Growth Zones in Eclogite Garnet," *J. Metamorph. Geol.* **20**, 769-780 (2002).
8. L. S. Darken, "Diffusion, Mobility, and Their Interrelation through Free Energy in Binary Metallic Systems," *Am. Inst. Miner. Metall. Eng. Trans.* **175**, 184-201 (1948).
9. N. L. Dobretsov and A. G. Kiryashkin, "The Dynamics of Subduction Zones: Models of Accretion Wedge Formation and Uplift of Glaucophane Schists and Eclogites," *Geol. Geofiz.*, No. 1, 3-16 (1992).
10. S. Duchene, J.-M. Lardeaux, and F. Albarede, "Exhumation of Eclogites: Insight from Depth-Time Analysis," *Tectonophysics* **280**, 125-140 (1997).
11. P. Erdmer, "Blueschists and Eclogite in Mylonitic Allochthons, Ross River and Watson Lake Areas, South-eastern Yukon," *Can. J. Earth Sci.* **24**, 1439-1449 (1987).
12. P. Erdmer and H. Helmstaedt, "Eclogite from Central Yukon: A Record of Subduction at the Western Margin of Ancient North America," *Can. J. Earth Sci.* **20**, 1389-1408 (1983).
13. P. Erdmer, E. D. Ghent, D. A. Archibald, and M. Z. Stout, "Paleozoic and Mesozoic High-Pressure Metamorphism

- at the Margin of the Ancestral North America in Central Yukon," *Geol. Soc. Am. Bull.* **110**, 615–629 (1998).
14. W. G. Ernst, J. L. Mosenfelder, M. L. Leech, and J. Liu, "H<sub>2</sub>O Recycling during Continental Collision: Phase Equilibrium and Kinetic Considerations," in *When Continents Collide: Geodynamics and Geochemistry of Ultrahigh-Pressure Rocks*, Ed. by B. R. Hacker and J. G. Liou (Kluwer, Dordrecht, 1998), pp. 275–295.
  15. J. Escartin, G. Hirth, and B. Evans, "Strength of Slightly Serpentinized Peridotites: Implications for the Tectonics of Oceanic Lithosphere," *Geology* **29**, 1023–1026 (2001).
  16. J. Ganguly, W. Cheng, and S. Chakraborty, "Cation Diffusion in Aluminosilicate Garnets: Experimental Determination in Pyrope–Almandine Diffusion Couples," *Contrib. Mineral. Petrol.* **131**, 171–180 (1998).
  17. D. Gebauer, H.-P. Schertl, M. Brix, and W. Schreyer, "35 Ma Old Ultrahigh-Pressure Metamorphism and Evidence for Very Rapid Exhumation in the Dora Maira Massif, Western Alps," *Lithos* **41**, 5–24 (1997).
  18. V. Yu. Gerasimov, "An Experimental Study of Iron–Magnesium Interaction in Garnets," *Dokl. Akad. Nauk SSSR* **295** (3), 684–688 (1987).
  19. T. V. Gerya and B. Stoeckert, "Exhumation Rates of High Pressure Metamorphic Rocks in Subduction Channels: The Effect of Rheology," *Geophys. Res. Lett.* **29**, 102-1–102-4 (2002).
  20. T. V. Gerya and D. A. Yuen, "Rayleigh–Taylor Instabilities from Hydration and Melting Propel 'Cold Plumes' at Subduction Zones," *Earth Planet. Sci. Lett.* **212**, 47–62 (2003).
  21. T. V. Gerya, B. Stockert, and A. L. Perchuk, "Exhumation of High-Pressure Metamorphic Rocks in Subduction Channel: A Numerical Simulation," *Tectonics* **21**, Art. N 1056, 6-1–6-19 (2002).
  22. E. D. Ghent, M. Z. Stout, P. M. Black, and P. M. Brothers, "Chloritoid-Bearing Rocks Associated with Blueschists and Eclogites, Northern New Caledonia," *J. Metamorph. Geol.* **5**, 239–254 (1987).
  23. M. T. Gomez-Pugnaire, L. Karsten, and V. Lopez Sanchez-Vizcaino, "Phase Relations and *P–T* Conditions of Coexisting Eclogite–Blueschists and Their Transformation to Greenschists: Facies Rocks in the Nerkau Complex Northern Urals," *Tectonophysics* **276**, 195–216 (1997).
  24. S. Guillot, K. H. Hattori, and J. Sigoyer, "Mantle Wedge Serpentinization and Exhumation of Eclogites: Insight from Eastern Ladakh, Northwest Himalayas," *Geology* **28**, 199–202 (1999).
  25. V. L. Hansen, M. T. Heizler, and T. M. Harrison, "Mesozoic Thermal Evolution of the Yukon–Tanana Composite Terrane: New Evidence from <sup>40</sup>Ar/<sup>39</sup>Ar Data," *Tectonics* **10**, 51–76 (1991).
  26. K. J. Hsu, "Franciscan Melange as a Model for Eugeosynclinal Sedimentation and Underthrusting Tectonics," *J. Geophys. Res.* **76**, 1162–1170 (1971).
  27. N. N. Kalitkin, *Numerical Methods* (Nauka, Moscow, 1978) [in Russian].
  28. A. C. Lasaga, "Multicomponent Exchange and Diffusion in Silicates," *Geochim. Cosmochim. Acta* **3**, 455–469 (1979).
  29. T. P. Loomis, J. Ganguly, and S. C. Elphick, "Experimental Determination of Cation Diffusivities in Aluminosilicate Garnets: II. Multicomponent Simulation and Tracer Diffusion Coefficients," *Contrib. Mineral. Petrol.* **90**, 45–51 (1985).
  30. L. Onsager, "Theories and Problems of Liquid Diffusion," *Ann. N. Y. Acad. Sci.* **46**, 241–265 (1945).
  31. S. Peacock, "Numerical Simulation of Metamorphic Pressure–Temperature–Time Paths and Fluid Production in Subduction Slabs," *Tectonics* **9**, 1197–1211 (1990).
  32. A. L. Perchuk, "A New Version of Omphacite–Albite–Quartz Geobarometer Considering Structural States of Omphacite and Albite," *Dokl. Akad. Nauk SSSR*, 324 (6), 1286–1289 (1992).
  33. A. L. Perchuk, "Eclogites of the Bergen Arcs Complex, Norway: Petrology and Mineral Chronometry," *Petrologiya* **10** (2), 115–136 (2002) [*Petrology* **10** (2), 99–118 (2002)].
  34. A. L. Perchuk and P. Philippot, "Geospeedometry and Timescales of High Pressure Metamorphism," *Int. Geol. Rev.* **42**, 207–223 (2000).
  35. A. L. Perchuk and P. Philippot, "Nascent Subduction: A Record in the Yukon Eclogites," *Petrologiya* **8** (1), 3–21 (2000) [*Petrology* **8** (1), 1–18 (2000)].
  36. A. L. Perchuk and D. V. Varlamov, "A New Type of the Prograde Heterogeneity of Garnet: Evidence from Eclogites of the Great Caucasus," *Geokhimiya*, No. 9, 1296–1310 (1995).
  37. A. L. Perchuk, V. Yu. Gerasimov, and P. Philippot, "Theoretical Modeling of Eclogite Uplift," *Petrologiya* **4** (5), 518–532 (1996) [*Petrology* **4** (5), 480–492 (1996)].
  38. A. L. Perchuk, P. Philippot, P. Erdmer, and M. Fialin, "Rates of Thermal Equilibration at the Onset of Subduction Deduced from Diffusion Modeling of Eclogitic Garnets, Yukon–Tanana Terrain," *Geology* **27**, 531–534 (1999).
  39. P. Philippot, J. Blichert-Toft, A. L. Perchuk, *et al.*, "Lu–Hf and Ar–Ar Geochronology Confirms Extreme Rate of Subduction Zone Metamorphism Deduced from Geospeedometry," *Tectonophysics* **342**, 23–38 (2001).
  40. D. J. Prior, J. Wheeler, F. E. Brenker, *et al.*, "Crystal Plasticity of Natural Garnet: New Microstructural Evidence," *Geology* **28**, 1003–1006 (2000).
  41. E. K. Ravna, "The Garnet–Clinopyroxene Fe<sup>2+</sup>–Mg Geothermometer: An Updated Calibration," *J. Metamorph. Geol.* **18**, 211–219 (2000).
  42. T. Reinecke, "Prograde High- and Ultrahigh-Pressure Metamorphism and Exhumation of Oceanic Sediments at Lago Di Cignana, Zermatt–Sass Zone, Western Alps," *Lithos* **42**, 147–189 (1998).
  43. D. Rubatto and J. Hermann, "Exhumation as Fast as Subduction?," *Geology* **29**, 3–6 (2001).
  44. E. K. H. Salje, "Thermodynamics of Sodium Feldspar: I. Order Parameter Treatment and Strain Induced Coupling Effects," *Phys. Chem. Miner.* **12**, 93–98 (1985).
  45. M. W. Schmidt and S. Poli, "Experimentally Based Water Budgets for Dehydrating Slabs and Consequences for Arc Magma Generation," *Earth Planet. Sci. Lett.* **163**, 361–379 (1998).

46. C. S. Schwandt, R. T. Cygan, and H. R. Westrich, "Ca Self-Diffusion in Grossular Garnet," *Am. Mineral.* **81**, 448–451 (1996).
47. M. G. Steltenpohl, Z. Cymerman, E. J. Krogh, and M. J. Kunk, "Exhumation of Continental Basement during Variscan Lithospheric Delimitation and Gravitation Collapse, Sudety Mountains, Poland," *Geology* **21**, 1111–1114 (1993).
48. Y. Tatsumi, "Origin of Subduction Zone Magmas Based on Experimental Data," in *Advances in Physical Geochemistry*, Vol. 9: *Physics and Chemistry of Magmas*, Ed. by L. L. Perchuk and I. Kushiro (Springer Verlag, New York, 1991), pp. 268–301.
49. D. Templeman-Kluit, "Transported Cataclasite, Ophiolite, and Granodiorite in Yukon: Evidence of Arc-Continent Collision," *Geol. Surv. Can.*, Paper 79-14 (1979).
50. H. L. Toor, "Solution of the Linearized Equations of Multicomponent Mass Transfer: II. Matrix Methods," *J. Am. Inst. Chem. Eng.* **8**, 460–465 (1964).
51. B. Wudner and W. Schreyer, "Antigorite: High-Pressure Stability in the System MgO–SiO<sub>2</sub>–H<sub>2</sub>O (MSH)," *Lithos* **41**, 213–227 (1997).
52. V. O. Yapaskurt, "Chemical Zoning of Minerals in Metamorphic Rocks: Evidence from Garnets of the Kokchetav Massif, Northern Kazakhstan," *Vestn. NSO Geol. Fac. Mosk. Gos. Univ.*, 59–63 (1997).